

Robust evolution system for Numerical Relativity

A. Arbona, C. Bona, J. Massó and J. Stela
Departament de Física. Universitat de les Illes Balears.
E-07071 Palma de Mallorca, SPAIN

Abstract

The paper combines theoretical and applied ideas which have been previously considered separately into a single set of evolution equations for Numerical Relativity. New numerical ingredients are presented which avoid gauge pathologies and allow one to perform robust 3D calculations. The potential of the resulting numerical code is demonstrated by using the Schwarzschild black hole as a test-bed. Its evolution can be followed up to times greater than one hundred black hole masses.

04.20.Ex, 04.25.Dm

arXiv:gr-qc/9902053v2 3 Mar 1999

I. INTRODUCTION

In spite of the valuable work made by many Numerical Relativity groups all around the world, three-dimensional (3D) gravitational systems are still challenging (see Ref [1] for a recent review of the field) . This is not only because the present generation of computers does not allow yet to perform high resolution 3D calculations. This is also, or at least we believe it is, because there are new numerical problems associated with 3D gravitational calculations which were not recognized in the previous work with spherically symmetric (1D) or even axially symmetric (2D) systems. To identify these new problems and to deal with them requires new developments, both from the theoretical and from the applied point of view.

The theoretical developments, as presented in Section II, are made in the framework of the well known 3+1 formalism [2–4]. We propose first to change the standard set of evolution equations (obtained from the space components of the four-dimensional Ricci tensor) to the one obtained from the space components of the Einstein tensor (which we called 'Einstein system' [5] for obvious reasons).

We will now incorporate to this second-order system the idea of transforming the momentum constraint into an evolution equation for a set of three supplementary quantities, which we used in former works with first-order evolution systems [6,7]. Although the original idea was devised to obtain hyperbolic evolution systems, variants of the same approach have been considered recently [8–10] as a tool to improve the results in specific numerical simulations.

These modifications do change completely the causal structure of the original system, as discussed in Refs [6,7]. The ones presented in Section III, on the contrary, are minor changes from the theoretical point of view but they seem to be crucial from the computational one. They address the problem of the so called 'gauge pathologies' [11,12], which consists in the explosive behaviour of the quantities associated with the gauge modes. This problem seldom happened in 1D calculations (at least for the standard settings) but, in our experience, it turns out to be the rule in 3D calculations.

A possible remedy to this problem could be trying to fix the gauge-related degrees of freedom by using the well known maximal slicing [13]. This requires, however, to solve a 3D elliptic equation at every time step, which implies a huge computational cost, specially in high resolution calculations. But this is not the only alternative available: the gauge-related degrees of freedom can be isolated from the rest of the system by using the well known conformal decomposition of the space metric [2,14] as in the recent work of Shibata and Nakamura [8], which use the harmonic slicing [15,16], which is much less expensive from the computational point of view.

Both alternatives, however, are not sufficient by themselves to allow for long term 3D calculations in strong field situations, like black hole space-times. Even if one tries to combine both approaches, the errors in gauge modes show a tendency to grow without bound which should be tackled using improved tools [10]. We have devised numerical counter-terms which have shown to be very effective in controlling these errors without modifying the analytical system of equations. As they are not restricted to maximal slicing, one is then allowed to use other slicings with a great increase in the code speed. The use of these counter-terms opens then the door to performing robust 3D numerical calculations at a level similar to

that of previous 2D or even 1D results.

We present in Section IV our results for the single black hole case as a test-bed for our finite difference code. We obtain long term evolution simulations, up to more than one hundred times the black hole mass. A convergence analysis shows that the collapse speed one obtains (the rate at which the numerical grid falls into the hole) depends on the grid resolution, but it converges to the well established results for spherically symmetric (1D) black holes. The same is true for the preservation of the black hole mass outside the horizon. A finer analysis, however, shows that the outer boundary conditions do not preserve the constraints and this affects the consistency of the long term results. In spite of that, the code runs forever (although we obviously stopped it when all the numerical grid fell into the hole).

II. SPACE PLUS TIME DECOMPOSITION

We will use the well known 3+1 decomposition [2–4] of the space-time metric, namely

$$ds^2 = -\alpha^2 dt^2 + \gamma_{ij} (dx^i + \beta^i dt) (dx^j + \beta^j dt) , \quad (1)$$

where the lapse function α and the shift β^i are related to the choice of the space-time coordinates and γ_{ij} is the induced metric on every time slice. The extrinsic curvature K_{ij} (second fundamental form) of the slices is given by

$$(\partial_t - \mathcal{L}_\beta) \gamma_{ij} = -2\alpha K_{ij} , \quad (2)$$

where \mathcal{L} stands for the three-dimensional Lie derivative operator.

Four of the ten Einstein field equations do not contain time derivatives when expressed in terms of the previously defined quantities. These four constraint equations can be easily identified: the “energy”, or Hamiltonian constraint

$$2\alpha^2 G^{00} = {}^{(3)}R - tr(K^2) + (tr K)^2 , \quad (3)$$

where ${}^{(3)}R$ is the trace of the three-dimensional Ricci tensor, and the “momentum constraint”

$$\alpha G^0_i = \nabla_k K^k_i - \partial_i(tr K) , \quad (4)$$

where index contractions and covariant derivatives are with respect to the induced metric γ_{ij} .

The time evolution of K_{ij} is given by a system obtained from the remaining Einstein field equations. For instance, the space components of the four-dimensional Einstein tensor can be written [5]

$$\begin{aligned} (\partial_t - \mathcal{L}_\beta) K_{ij} &= -\nabla_i \alpha_j + \\ &\alpha [{}^{(3)}R_{ij} - 2K_{ij}^2 + tr K K_{ij} - G_{ij}] \\ &- \alpha/4 \gamma_{ij} [{}^{(3)}R - tr(K^2) + (tr K)^2 - 2 tr G] , \end{aligned} \quad (5)$$

where ${}^{(3)}R_{ij}$ stands for the three-dimensional Ricci tensor. The matter terms in the perfect fluid case can be computed from

$$G_{ij} = 8\pi [(\mu + p)u_i u_j + p \gamma_{ij}] , \quad (6)$$

where μ is the total energy density of the fluid, p is the pressure, and u_i is its fluid 3-velocity.

We call this set of equations (2,5) the Einstein evolution system. Notice that it differs from the standard 3+1 evolution system (obtained from the space components of the four-dimensional Ricci tensor) by a term containing the Hamiltonian constraint. This ensures that the matter contribution (6) vanishes in the Newtonian limit. Even in the vacuum case, the Einstein evolution system has proved to be superior when following the long term evolution for a spherically symmetric (1D) black hole [5].

A. The momentum constraint as an evolution equation

Let us consider now the quantities V_i , which can be obtained from the metric first derivatives as follows

$$V_i \equiv 1/2 \gamma^{rs} (\partial_i \gamma_{rs} - \partial_r \gamma_{is}) . \quad (7)$$

One can alternatively compute the time evolution of V_i by using the momentum constraint (4) as a dynamical equation, that is [5]:

$$\begin{aligned} \partial_t V_i - \beta^k \partial_k V_i - (\partial_i \beta^r) V_r + \\ 1/2 (\gamma^{kr} \gamma_{is} - \delta_i^k \delta_s^r) \partial_{kr}^2 \beta^s = \\ \alpha^2 G_i^0 + \alpha_r K_i^r - \alpha_i \text{tr} K - \\ \alpha [2 K_i^r V_r + K^{rs} \Gamma_{irs} - K_i^r \partial_r (\ln \sqrt{\gamma})] . \end{aligned} \quad (8)$$

We have chosen this second approach, which amounts to consider the following set of basic dynamical quantities

$$\{\gamma_{ij} , K_{ij} , V_i\} , \quad (9)$$

so that the condition (7) can be now considered just as an algebraic constraint which will hold if and only if the momentum constraint is satisfied.

The three-dimensional Ricci tensor can be written in terms of these quantities as

$$\begin{aligned} {}^{(3)}R_{ij} = -1/2 \gamma^{rs} \partial_{rs}^2 \gamma_{ij} + \partial_{ij}^2 \ln \sqrt{\gamma} - \partial_i V_j - \partial_j V_i + \\ \Gamma_{ij}^k (2 V_k - \partial_k \ln \sqrt{\gamma}) + \gamma^{kl} \gamma^{rs} [(\partial_k \gamma_{ri})(\partial_l \gamma_{sj}) \\ - \Gamma_{ikr} \Gamma_{jls}] , \end{aligned} \quad (10)$$

so that its trace can be easily expressed as follows

$${}^{(3)}R = -2 \partial_k V^k + \Gamma_{krs} \Gamma^{rks} - \gamma^{rs} (\partial_r \ln \sqrt{\gamma}) (\partial_s \ln \sqrt{\gamma}) . \quad (11)$$

B. Gauge conditions

So far we have considered a completely general coordinate system. We will keep our freedom to fix the shift components β^i as purely kinematical quantities. The choice of the lapse function α , on the contrary, will be closely related with the dynamics of our system.

A popular choice is to impose the maximal slicing condition [13]

$$tr K = 0, \quad (12)$$

which amounts to compute α by solving the elliptic equation obtained by taking the trace of (5) or a combination of this trace with the Hamiltonian constraint (3). This choice has proven to be quite effective in some cases, although it is not free from long term instabilities. Also, elliptic equations are very expensive in terms of computational resources and getting high resolution long term calculations on three-dimensional grids seems to be beyond the capabilities of present day computers.

A different strategy is to link the evolution of the lapse α to that of the volume element $\sqrt{\gamma}$ by means of the following equation

$$(\partial_t - \mathcal{L}_\beta) \ln \alpha = -\alpha f tr K, \quad (13)$$

where f is a given non-negative function of α . This opens the way to many different choices of the time slicing. The geodesic slicing is included as a subcase with $f = 0$. The $f = 1$ case corresponds to the “harmonic slicing” [15,16] (the resulting time coordinate is harmonic). Another interesting case is obtained when $f = 1/\alpha$; it mimics maximal slicing near a singularity, when the lapse collapses to zero (a very similar case was considered in [18,19]). The related choices $f = n/\alpha$ ($n = 2, 4$) mimic both the singularity-avoidance and the large-gradients-avoidance properties of the maximal slicing for a fraction of the computational cost.

So far we have obtained a closed dynamical system (once the shift β^i is given) which can be considered as the second-order equivalent of the first-order hyperbolic system given in Ref [7,5]. The causal structure of this second-order system will be discussed elsewhere [17]. All we can say by now is that the direct equivalence with a first-order system which is known to be hyperbolic seems a good starting point for numerical relativity applications. But this feeling should be confirmed by experience, as we will see in what follows.

III. A ROBUST EVOLUTION SYSTEM

A. Keeping apart trace and trace-free components

Both from the theoretical and from the practical point of view [2,14], it is clear that $tr K$ is directly related to the gauge degrees of freedom, which should be treated very carefully to avoid spurious ‘gauge pathologies’ or riddles that do appear too frequently in 3D calculations [12]. This suggests the convenience of evolving separately the trace and trace-free components of K_{ij} .

We will follow here the notation of Shibata and Nakamura [8] to write down the following conformal decomposition of the space metric

$$\gamma_{ij} = e^{4\Phi} \tilde{\gamma}_{ij} \quad (14)$$

with Φ chosen so that the determinant $\tilde{\gamma}$ of the conformal metric is equal to unity, namely

$$\sqrt{\tilde{\gamma}} = e^{6\Phi} . \quad (15)$$

This means that we can split out the evolution equation (2) into the following pieces [20]:

$$(\partial_t - \mathcal{L}_\beta) \tilde{\gamma}_{ij} = -2\alpha A_{ij} , \quad (16)$$

$$(\partial_t - \mathcal{L}_\beta) \Phi = -1/6 \alpha K , \quad (17)$$

where we have noted for short

$$A_{ij} \equiv e^{-4\Phi} (K_{ij} - 1/3 \text{tr} K \gamma_{ij}) , \quad (18)$$

$$K \equiv \text{tr} K . \quad (19)$$

We can also split out the evolution equations (5, 8) in the same way:

$$\begin{aligned} (\partial_t - \mathcal{L}_\beta) A_{ij} = & e^{-4\Phi} \{ -\tilde{\nabla}_i \alpha_j + 2 (\alpha_i \Phi_j + \alpha_j \Phi_i) \\ & + 1/3 \tilde{\gamma}^{rs} (\tilde{\nabla}_r \alpha_s - 4 \alpha_r \Phi_s) \tilde{\gamma}_{ij} \\ & + \alpha [{}^{(3)}R_{ij} - 1/3 (\tilde{t}r {}^{(3)}R) \tilde{\gamma}_{ij} - G_{ij}] \} \\ & + \alpha (K A_{ij} - 2 \tilde{\gamma}^{rs} A_{ir} A_{js}) \end{aligned} \quad (20)$$

$$\begin{aligned} (\partial_t - \mathcal{L}_\beta) K = & e^{-4\Phi} \{ -(\tilde{\gamma}^{rs} \tilde{\nabla}_r \alpha_s) - 2 (\tilde{\gamma}^{rs} \alpha_r \Phi_s) \\ & + \alpha [1/4 \tilde{t}r {}^{(3)}R + 1/2 \tilde{t}r G] \} \\ & + \alpha (1/2 K^2 + 3/4 \tilde{\gamma}^{rs} \tilde{\gamma}^{kl} A_{kr} A_{ls}) , \end{aligned} \quad (21)$$

$$\begin{aligned} \partial_t V_i - \beta^k \partial_k V_i - (\partial_i \beta^r) V_r + 1/2 (\tilde{\gamma}^{kr} \tilde{\gamma}_{is} - \delta_i^k \delta_s^r) \partial_{kr}^2 \beta^s \\ = \alpha^2 G_i^0 + A_{ir} \tilde{\gamma}^{rs} (\alpha_s - 2\alpha V_s + 2\alpha \Phi_s) \\ - \alpha \tilde{\gamma}^{kr} \tilde{\gamma}^{ls} A_{kl} \tilde{\Gamma}_{irs} - 2/3 K \alpha_i . \end{aligned} \quad (22)$$

The resulting system (16, 17, 20, 21, 22) allows to compute the time evolution of the enlarged set of dynamical quantities

$$\{ \tilde{\gamma}_{ij} , \Phi , A_{ij} , K , V_i \} , \quad (23)$$

which has the same basic structure of the Einstein evolution system (2, 5, 8) because the two extra quantities we have introduced are redundant, so that the constraints

$$\det \tilde{\gamma} = 1 , \quad \tilde{t}r A = 0 \quad (24)$$

are trivially propagated in time.

B. Numerical counter-terms

In numerical applications the algebraic constraints (24) can be easily monitored as error indicators. Their behaviour is quite unstable: $\tilde{tr} A$ grows without bound (the actual rate depends on every case) and this makes $\det \tilde{\gamma}$ to go far away of its exact value of 1. This leads to an obvious inconsistency which causes the numerical 3D code to crash after a relatively short time.

To fight against these errors, we have modified the right-hand-sides of the evolution equations (16, 20) by adding the following counter-terms:

$$(\partial_t - \mathcal{L}_\beta) \tilde{\gamma}_{ij} = \dots - 1/3 (\det \tilde{\gamma} - 1)/\tau \tilde{\gamma}_{ij} , \quad (25)$$

$$(\partial_t - \mathcal{L}_\beta) A_{ij} = \dots - 1/3 (\tilde{tr} A)/\tau \tilde{\gamma}_{ij} , \quad (26)$$

where τ is a 'time constant'.

It is easy to see that the counter-terms (25, 26) by themselves would cause an exponential decrease of the errors in $\tilde{tr} A$ and $\det \tilde{\gamma}$. In practice, we have set the time constant τ to the same value of the numerical time step dt in order to keep these errors within an small order of magnitude.

One should notice at this point that these counter-terms do vanish in the continuum limit (at least for second-order-accurate numerical algorithms), so that they do not affect at all the structure of the analytical evolution system. Harmless from the theoretical point of view, they provide a valuable tool that allows us to perform robust 3D calculations, as we will see below. See Refs. [21,22] for the use of numerical control terms in elliptic gauge conditions.

IV. APPLICATION TO THE BLACK HOLE CASE

Let us start with the usual time symmetric initial data ($K_{ij} = 0$) for a conformally flat metric (space isotropic coordinates), corresponding to a Schwarzschild black hole. Let us now replace the interior region by a constant density incoherent matter content, keeping the exterior vacuum region of the original hole [23]. This 'stuffed' black hole approach allows one to start from singularity-free initial data and avoids then the usual procedure of excising the inner region from the computational grid, which would introduce an internal boundary at the black hole horizon.

We have performed our calculations in the Cactus code [1] environment. In order to save computational resources, we have taken advantage of the equatorial symmetry of the problem to evolve just an octant of the space slices. This requires to introduce boundary conditions at the symmetry planes. The outer boundary has been treated as in Ref [8]. In Fig. 1 we consider the effect of this boundary condition over the collapse of the lapse. The results seem to be quite independent on the position of the outer boundary.

FIGURES

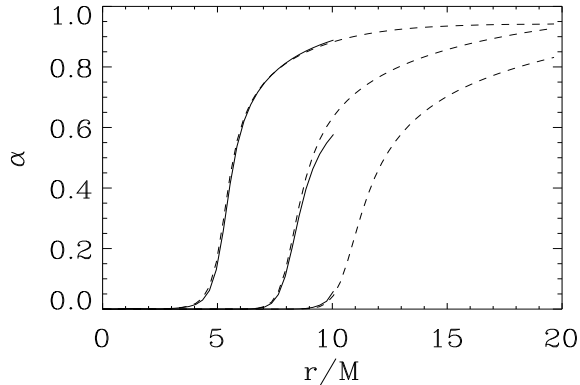


FIG. 1. The evolution of α is compared for two positions of the external boundary ($r = 10M$ and $r = 20M$) for a Schwarzschild black hole. The resolution is set at $dx = 0.3M$. The lapse is plotted at $t = 27M$, $37M$ and $47M$. In the latter the black hole has gone almost out of the smallest grid. We can see that the agreement is quite good.

As coordinate conditions, we use normal coordinates ($\beta^i = 0$) and an algebraic slicing of the form (13) with the choice $f = 2/\alpha$ which leads to smoother profiles of the evolved quantities. To start a dynamical simulation we can take as usual a constant initial lapse. The time evolution is then obtained by using the 'icn' second-order-accurate algorithm which has been incorporated to the Cactus version currently used by the Potsdam group. The actual plight for the reliability of this collapse turns out to be resolution, as we can see in Fig. 2. The 3D results converge to the well established 1D solution and we see that a resolution finer than $0.1M$ is needed if one wants to get really close to the physical solution.

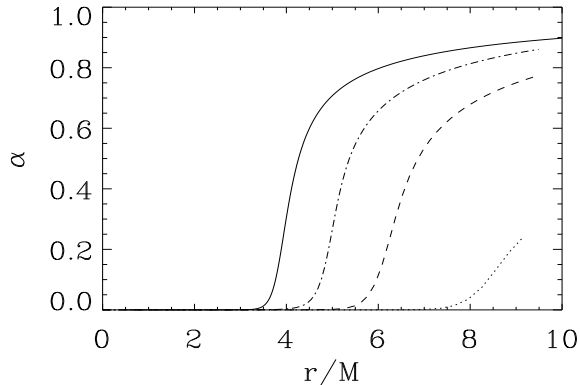


FIG. 2. The convergence of the lapse towards 1D results is shown. α is plotted against r/M at $t = 30M$ for a Schwarzschild black hole. The solid line corresponds to the 1D result with high resolution. The remaining lines, converging to that solution, correspond to 3D results with $dx = 0.3M$, $0.15M$ and $0.075M$.

As far as our test-bed problem has spherical symmetry, we can make use of the Bondi mass function to monitor the convergence of the numerical solution towards the analytical one. In Fig. 3 we plot the time evolution of the numerically obtained mass at the apparent horizon. The results show the expected convergence to the constant line corresponding to the analytical value. This confirms our previous conclusions.

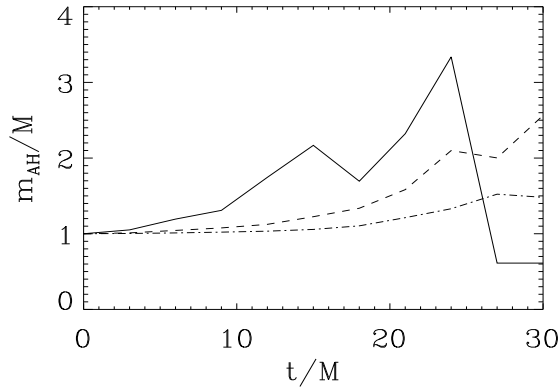


FIG. 3. The Bondi mass at the apparent horizon is plotted against time for a Schwarzschild black hole. Results with three resolutions ($dx = 0.3M$, $0.15M$ and $0.075M$) are plotted, which show convergence to the analytical value $m_{AH}/M = 1$.

Finally, we show in Fig. 4 the performance of the code in long runs. We can follow the black hole evolution for unlimited time. We just stop the calculation when the numerical grid is almost completely inside the hole.

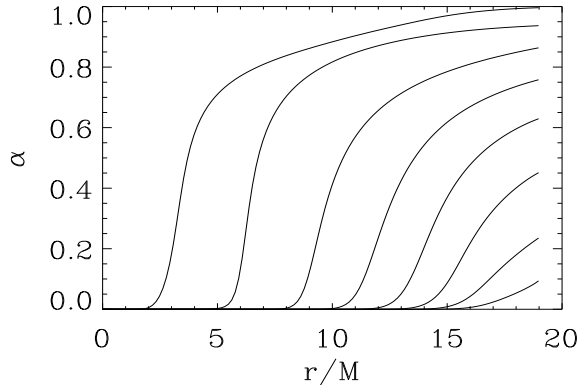


FIG. 4. The collapse of the lapse for a Schwarzschild black hole is shown. α is plotted against the radius for increasing times ($t = 15M$, $30M$, $45M$, $60M$, $75M$, $90M$, $105M$, $120M$). The whole grid goes eventually inside the hole and the calculation is stopped (although it never crashes). At late times, however, the numerical solution departs from the physical one due to boundary effects.

V. CONCLUSIONS

The equations we propose are interesting both from the theoretical and for the numerical point of view. The decomposition of K_{ij} into trace and trace-free parts allows a separate monitoring of the numerical errors which leads to the following quite surprising conclusion: the numerical trace of the trace-free part becomes easily unstable in strong field 3D calculations. Notice that this decomposition is not made in most Numerical Relativity formalisms, so that the errors arising from the trace-free part are directly mixed up with the dynamics of the trace part. This might explain the arising of the so called 'gauge pathologies' [11,12] even in situations with apparently harmless initial data.

The counter-terms we have introduced allow one to deal with this problem and this is enough to perform robust 3D Numerical Relativity calculations, even in the black hole case. We have demonstrated this by actually running the code up to times greater than one hundred black hole masses without any sign of instability: we just stopped when nearly all the numerical grid was inside the hole.

ACKNOWLEDGMENTS

This work is supported by the Dirección General para Investigación Científica y Técnica of Spain under project PB97-0134 and the Conselleria d'Educació, Cultura i Esports of the Balearic Government under an A7 grant.

We want to thank the Numerical Relativity groups of the Albert Einstein Institute in Potsdam and the Washington University (headed by Edward Seidel and Wai-Mo Suen, respectively) for useful discussions and for allowing comparison with their own data. Special thanks are due to Miguel Alcubierre and Bernd Bruegmann for providing access to limited access software tools in the Cactus code environment which have been used to speed up our code development.

REFERENCES

- [1] C. Bona, J. Massó, E. Seidel and P. Walker, gr-qc/9804052.
- [2] A. Lichnerowicz, J. Math. Pures Appl. **23**, 37 (1944).
- [3] Y. Choquet-Bruhat, in *Gravitation: an introduction to Current Research*, ed. L. Witten (Wiley, New York, 1962).
- [4] R. Arnowitt, S. Deser and C. W. Misner, in *Gravitation: an introduction to Current Research*, ed. L. Witten (Wiley, New York, 1962).
- [5] C. Bona, J. Massó, E. Seidel and J. Stela, Phys. Rev. **D56**, 3405 (1997).
- [6] C. Bona and J. Massó, Phys. Rev. Lett. **68**, 1097 (1992).
- [7] C. Bona, J. Massó, E. Seidel and J. Stela, Phys. Rev. Lett. **75**, 600 (1995).
- [8] M. Shibata and T. Nakamura, Phys. Rev. **D52**, 5428, (1995).
- [9] T. Baumgarte and S. Shapiro, Phys. Rev. **D59** (1999) 024007.
- [10] M. Alcubierre et al, Gravitational Collapse of Gravitational Waves in 3D Numerical Relativity, in preparation.
- [11] M. Alcubierre, Phys. Rev. **D55**, 5981, (1997).
- [12] M. Alcubierre and J. Massó, Phys. Rev. **D57**, 4511, (1998).
- [13] J. W. York Jr., Phys. Rev. Lett. **28**, 1082 (1972).
- [14] J. W. York Jr., Phys. Rev. Lett. **26**, 1656 (1971).
- [15] Y. Choquet-Bruhat and T. Ruggeri, Comm. Math. Phys. **89**, 269 (1983).
- [16] C. Bona and J. Massó, Phys. Rev. **D38**, 2419, (1988).
- [17] M. Alcubierre et al., in preparation.
- [18] A. Abrahams, D. Bernstein, D. Hobill, E. Seidel and L. Smarr, Phys. Rev. **D45**, 3544 (1992).
- [19] P. Anninos, D. Hobill, E. Seidel L. Smarr and W.-M. Suen, Phys. Rev. Lett. **D71**, 2851 (1993).
- [20] Notice that $\Phi, \tilde{\gamma}_{ij}, A_{ij}$ are three-dimensional tensorial densities (not tensors!) and the corresponding Lie derivatives must be computed accordingly.
- [21] J. Balakrishna, G. Daues, E. Seidel, W. Suen, M. Tobias and E. Wang, Class. Quant. Grav. 13 (1996) L135-L142
- [22] *Sources of Gravitational Radiation*, edited by L. Smarr (Cambridge University Press, Cambridge, England, 1979)
- [23] A. Arbona et al. Phys. Rev. **D57**, 2397, (1998).